PHYSICAL REVIEW A VOLUME 15, NUMBER 4 APRIL 1977

Collisional-radiative transfer between Rydberg states of helium and electronic recombination of He^+

J. Boulmer, F. Devos, J. Stevefelt,* and J-F. Delpech

Groupe d'Electronique dans les Gaz, Institut d'Electronique Fondamentale, Bâtiment 220, Université Paris-XI, Centre d'Orsay, 91405, Orsay, France

(Received 2 August 1976)

We report detailed spectroscopic measurements of light emission and excited level populations in a pure-helium afterglow at a pressure of 2.03 Torr. The free-electron temperature could be varied by microwave heating. Electron density n_e and temperature T_e were measured by precision microwave interferometry and they range from 5×10^9 to 3×10^{11} cm^{-3} for n_e and from 300 to 600°K for T_e. Rydberg states of neutral helium near the bottleneck for collisional-radiative (CR) recombination were perturbed in a well-controlled manner by photoionization with 10.6-μm photons. Our experimental data are consistent with a CR recombination scheme with simultaneous stabilization by collisions with free electrons and with neutral helium atoms. They establish the fact that the Gryziński formalism for electron-impact-induced transitions between bound rydberg states of high principal quantum number seriously overestimates the probability of collisions with small energy transfers. This study gives also experimental indications of what appears to be neutral-stabilized CR recombination of an atomic ion, He^+. The experimental recombination rate coefficient is well represented over the range of parameters covered at 2.03 Torr by $\alpha(\text{cm}^3\ \text{sec}^{-1}) = 3.5\times10^{-5}\,T_e^{-1.9} + 6.0\times10^{-9}\,T_e^{-2.18}\,n_e^{0.37} + 3.8\times10^{-9}\,T_e^{-4.5}\,n_e$, in reasonable agreement with available theories.

I. INTRODUCTION

In a recent paper[1] (hereafter referred to as I), we theoretically investigated the electron-ion three-body collisional-radiative (CR) recombination in cold plasmas, where the third body is an electron. We used the Mansbach and Keck[2] transition rates between hydrogenic levels of high principal quantum numbers. These classical rates involve a minimum of hypotheses and were derived under approximations which may be expected to be well verified in a cold helium plasma; they should be correct in the classical limit, even for small energy transfers.

The results of these calculations were indeed found to be in good agreement with experimental data for e-He^+ recombination. However, as seen in Fig. 2 of I, the available experimental determinations of the CR recombination rate exhibit a marked scatter, and it is difficult to draw from them significant conclusions concerning the applicability of our theory or of the theories of Bates *et al.*[3] and of Johnson and Hinnov.[4]

It thus appeared desirable to obtain detailed measurements in a well controlled helium afterglow, where the electron temperature and density could be independently varied and precisely measured.[5] Of additional interest was the fact that when the degree of ionization is very low, three-body collisions with a neutral atom should play a role in stabilizing the electron-ion recombination, despite the small electron/neutral mass ratio. In fact, theoretical estimates[6] show that this process may become important for ionization degrees between 10^{-6} and 10^{-7} in helium at temperatures between 300 and 600°K. One should thus expect to encounter different energy-transfer and recombination mechanisms over a range which can be easily covered in a stationary helium afterglow plasma at filling pressures of a few Torrs. We have accordingly measured by spectroscopic methods the e-He^+ recombination rate coefficient in these temperature and density ranges.

However, as seen in I, the over-all recombination rates turn out to be relatively insensitive to the actual transition rates between levels. An unambiguous choice of a set of transition rate coefficients is not possible, even with precise empirical observations of the recombination rate coefficient alone. It was thus felt necessary to complement these observations by the study of a physical phenomenon which would be more sensitive to the transition rates between energy levels in the vicinity of the "bottleneck" in the CR recombination sequence (the bottleneck concept is discussed in some detail in I). This is the case with the quenching of plasma light emission induced by the irradiation of a recombining plasma with photons near 10.6 μm produced by a CO_2 laser of moderate power density, as was first demonstrated by Kaplafka, Merkelo, and Goldstein.[7] Irradiation leads to photoionization of the energetically accessible levels of principal quantum number $p \geq 11$ and to depletion of the excited state populations near the bottleneck, and thus constitutes a precise, selective perturbation technique.

We shall first briefly complement the theory of I by examining some theoretical aspects of the

perturbation of a recombining plasma by far-infrared radiation, and by showing that it allows a reasonably sensitive determination of the actual value of the rates to be used for the collision-induced transitions between energy levels. We shall then describe our experimental investigations in a helium afterglow plasma under closely controlled conditions, with and without infrared laser irradiation.

II. THEORY OF THE PERTURBATION OF A RECOMBINING PLASMA BY INFRARED IRRADIATION

The effect of irradiating a recombining helium plasma with infrared light from a CO_2 laser (10.6 μm wavelength) at a power density of the order 1 kW/cm^2 is limited to photoionization of high rydberg states. Other effects, such as photoexcitation, electron or neutral gas heating by infrared absorption or stimulated radiative capture are negligibly small.

The cross section for photoionization of the hydrogenic quantum level p by photons of energy $h\nu$ is

$$\sigma(p,h\nu)=\frac{64\alpha_{fs}\pi a_0^2}{3\sqrt{3}\,p^5}\left(\frac{\mathcal{R}}{h\nu}\right)^3 g(p,h\nu)\ , \tag{1}$$

where α_{fs} is the fine-structure constant, a_0 the Bohr radius, and $\mathcal{R}$ the rydberg energy. Near threshold and for high enough values of p, the Gaunt factor $g(p,h\nu)$ is very nearly unity in hydrogen, and Eq. (1) reduces to the classical Kramers cross section.[8]

In the model used in I, we lump together all singlet and triplet levels of helium of given p and of various orbital quantum numbers l into a single equivalent degenerate hydrogenic level of ionization energy $\mathcal{R}/p^2$. This approximation is justified in our context for the levels of importance for CR recombination ($p \gtrsim 7$), as the quantum defect is negligible for terms with large l which have dominant statistical weight, and as helium has only one ionization limit; the global Gaunt factor for photoionization of such an equivalent level should also be very close to unity.

The photoionization cross section scales as p^{-5} and hence it is the lowest energetically accessible level, i.e., $p=11$, which will be the most depleted directly by 10.6-μm irradiation; this quenching will be transferred essentially by electronic or neutral collisions to the other excited levels. For a correct treatment of these complex collisional-radiative processes, in the limit of purely electronic transfer, we should substract from the left-hand side of the rate equation (1) of I for all levels with $p \geq 11$ a term $P_{(p)}$ representing the number of photoionization events per unit time and volume

$$P_{(p)}=\sigma(p,h\nu)\times\Phi\times N_p\ , \tag{2}$$

where Φ is the infrared photon flux (number of photons per unit time and per unit surface) and N_p is the number density of quantum level p.

The corresponding system of rate equations was solved on a computer using the methods discussed in paper I, yielding the predicted relative quenching

$$Q_p=1-N_p^{(ir)}/N_p\ , \tag{3}$$

where $N_p^{(ir)}$ is the number density of quantum level p with infrared perturbation. Q_p is shown in Fig. 1 for a typical case for different quantum levels p. Whatever transfer rate coefficients are chosen, it is seen that quenching is strongest for the $p=11$ level, whereas all $p<11$ levels are quenched by the same amount, which corresponds to the reduction in the CR recombination cascade down from levels $p \geq 11$. For $p>11$ the quenching decreases rapidly because of the p^{-5} dependence of $\sigma(p,h\nu)$ combined with increasing collisional rates. As the collisional rates calculated in the Gryziński approximation[9] are much larger (by a factor ~20) than those obtained by Mansbach and Keck[2] for transitions around $p=11$, the corresponding quenching is smaller, as shown on Fig. 1.

Qualitatively—always in the limit of purely elec-

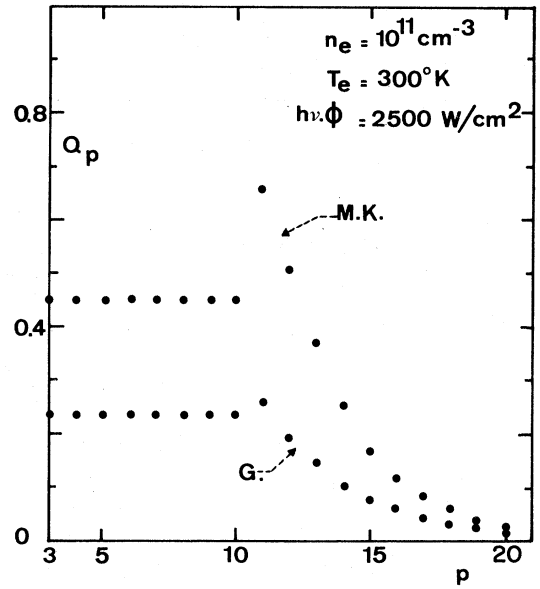

FIG. 1. Predicted relative quenching Q_p of excited level densities vs principal quantum number p due to 10.6-μm irradiation under typical experimental conditions for electron-stabilized collisional-radiative theories with Mansbach and Keck (MK) and Gryziński (G) rate coefficients. Quenching is maximum for the first energetically accessible level, $p=11$.

tronic transfer—a decrease in electron density or an increase in infrared photon flux will both result in an enhanced quenching since photoionization is essentially balanced against electron collisions. In fact, in the electron-stabilized collisional limit we find that for a given electron temperature the quenching Q_p is for any p and within 10% a unique function of the ratio $\zeta = h\nu\Phi/n_e$ for power fluxes $h\nu\Phi$ up to 5 kW cm^{-2} and for ζ up to 3×10^{10} W cm. In the experimentally important case of the $p=3$ level, for Mansbach and Keck collisional transfer rates,

$$Q_3 \cong 2.2\times10^{-8}\zeta\,[1-\exp(-4.0\times10^{7}\zeta^{-0.76})]T_e^{-1.1}\ . \tag{4}$$

When excitation transfers by neutral collisions become dominant, the quenching should become independent of electron density. As the corresponding transfer rates are poorly known, we have not attempted to make quantitative estimates of this effect.

By means of infrared perturbation techniques, it will thus be possible to distinguish between different sets of electron or neutral impact transition rate coefficients, and to monitor the transition between electron-stabilized and neutral-stabilized collisional recombination. The corresponding experimental results are deferred to Sec. IV D.

III. EXPERIMENTAL EQUIPMENT AND METHODS

A block diagram of the experimental system is shown in Fig. 2. The discharge was created in a 50-cm-long, 8.0-mm-i.d. quartz tube; its central part was 30 cm long. Germanium windows, transparent to the 10.6-μm radiation, were provided at both ends and were nearly perpendicular to tube axis; they were soldered to the quartz tube through a quartz–Pyrex–Kovar–stainless-steel–titanium graded seal. The central part of the tube was located inside a standard X-band waveguide (inside cross section 10.16×22.86 mm^2). The light emitted by the plasma was observed through a slit in the waveguide (length 83 mm, width 2 mm).

The discharge pulse was applied to two electrodes situated outside the tube axis and near its ends. Pulse duration was 50 μsec, with a current ~200 mA, at a repetition rate of 200 sec^{-1}. During the afterglow period, the voltage between the electrodes was clamped to zero to avoid perturbing the free electrons. All experiments (unless otherwise stated) were performed at a helium filling pressure of 2.03 ± 0.03 Torr at room temperature (nominally 300 °K). Gas heating by the discharge pulse was negligible.

The discharge tube was connected to a high-vacuum system. High-purity helium gas provided by l'Air Liquide in 1-liter metal flasks was used; it was further purified in a cataphoresis tube during 48 h before being introduced into the discharge tube. During operation of the discharge, impurities released from walls and electrodes were continuously removed by a getter pump. The system was baked at 200 °C during 24 h; this was the maximum rated temperature of the germanium windows. After baking, pressure rise was below a few 10^{-11} Torr liter sec^{-1}. The only impurity which could be detected spectroscopically was a small trace of hydrogen. An identical discharge tube, without germanium end windows, was baked at 400 °C for 24 h; all results (of course without 10.6-μm irradiation) were identical to those obtained in the present tube, with the only difference that traces of hydrogen could not be detected. We conclude that gas purity was sufficient, even with the moderate baking temperature of 200 °C.

The X-band microwave diagnostics system has been described elsewhere.[10] It operates at a frequency of 8.77 GHz; probe power is about 1 μW.

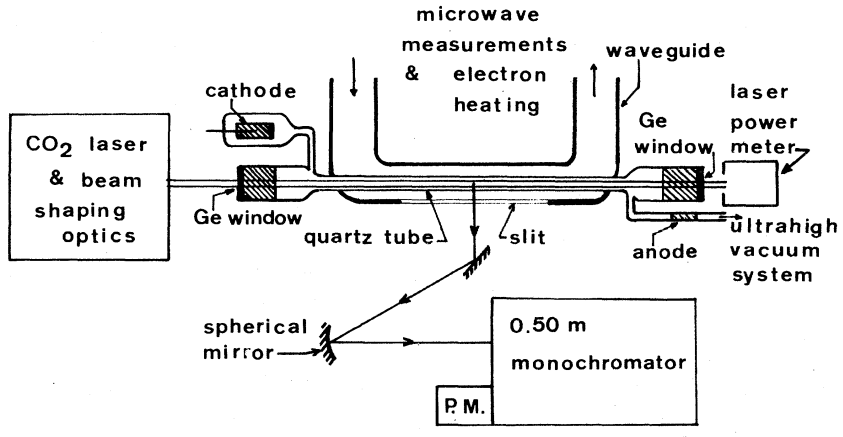

FIG. 2. Block diagram of the experimental system.

The microwave interferometer was calibrated by replacing the discharge tube by an identical quartz tube which could be filled with gases of known dielectric coefficient (CO_2, N_2, and He) at pressures up to 1 atm. The absolute determination of electron temperatures by radiometry or from collision-frequency measurements[11] becomes extremely difficult at low helium pressures. We shall see in Sec. IV A that electron temperature could be directly inferred from measurements of ambipolar diffusion loss rates.

The light emitted along the diameter of the plasma column through the slit in the waveguide was focused by a system of mirrors on the entrance slit of a 0.5-m holographic grating spectrometer. On the exit side, we used a RCA C31034 photomultiplier tube in the photon counting mode; the photocathode quantum efficiency is above 10% in the wavelength interval between 2300 and 8200 Å. Dark noise was kept below 50 counts/sec by cooling to $-40\,^{\circ}C$. To conserve low noise and high sensitivity in the late afterglow, the photomultiplier tube was protected from the intense light emission during the discharge and the early afterglow by clamping the first two dynodes to the photocathode potential during the first 100 μsec of each discharge cycle. The optical-electronic system was carefully calibrated for absolute intensity measurements against a tungsten-ribbon filament lamp, itself calibrated by the Bureau National de Métrologie in Paris.

Two different perturbation techniques were used to obtain information about the recombination processes. The now classical method of selective electron heating by a low-power microwave field[12] was employed to study the influence of electron temperature. The microwave heating field (*X* band, 9.20 GHz) could be applied during any preselected time interval in the afterglow; to avoid transient phenomena, it began always at least 50 μsec before the start of the measurement period. Three different heating power were used: 12, 24, and 38 mW. The electron temperature increment can be related quite precisely to the microwave power.[13] In this geometry and taking the quartz tube into account, the computed proportionality factor is $4.58\,^{\circ}K\,mW^{-1}$.

In addition we have used the perturbation method first described by Kaplafka *et al.*[7] A pulsed laser was used to photoionize excited levels near the "bottleneck" of the CR recombination sequence. The CO_2 laser which we built and used had a pulse duration between 10 and 150 μsec at a maximum pulse rate of 100 pulses/sec with a pulse energy typically between 10 and 20 mJ. The laser beam was made parallel and adjusted to a diameter between 2 and 6 mm by means of spherical gold-coated mirrors before entering the discharge tube. By varying the beam diameter and/or inserting attenuating filters, the irradiation intensity could be varied from 50 to 2000 W/cm^2. Spatial and temporal variations of the laser pulse were monitored with a rapid pyroelectric detector, while the total energy was measured with a precision calorimeter. Reflections and attenuations due to the germanium entrance and exit windows were taken into account, and extreme care was exercised to obtain a meaningful absolute evaluation of the time- and space-resolved infrared photon flux inside the plasma.

Experimental data were accumulated in three 32-channel analyzers. It was thus possible to measure simultaneously laser power, plasma light emission on a spectral line, and its variation due to laser perturbation, all with a time resolution of 1 μsec (channel widths of 10 or 20 μsec were used in practice). An individual experimental run comprised up to 2^{18} discharges and lasted more than 20 min. The corresponding lower sensitivity limit for light intensity measurements corresponds to about one detected photon every 2000 discharges. The measured values for each channel were punched on paper tape for subsequent digital treatment by a computer. The whole experimental system was reproducible within error bars over the span of several months necessary to gather the data presented in Sec. IV.

IV. EXPERIMENTAL RESULTS

A. Free-electron number density and temperature

No measurements were taken during the early afterglow, i.e., less than 100 μsec after the end of the discharge pulse, to avoid complicated transient phenomena.

The electron density during the afterglow is a function both of time and of radial position inside the container. It is the solution, with proper initial and boundary conditions, of a nonlinear, partial differential equation including losses by ambipolar diffusion and by recombination and a source term describing electron production during the afterglow, probably by metastable-metastable collisions.[5] This may be symbolically written

$$\left(\frac{dn_e}{dt}\right)_{\text{meas}} = \left(\frac{dn_e}{dt}\right)_{\text{diff}} + \left(\frac{dn_e}{dt}\right)_{\text{rec}} + \left(\frac{dn_e}{dt}\right)_{\text{source}} . \qquad (5)$$

Figure 3 shows the measured electron density at 2.03 Torr during the afterglow period of interest for the unperturbed plasma and for each of the three microwave heating fields applied during the whole of the afterglow. Systematic errors on electron density measurement are estimated to be below 4%. The decay is seen to be truly ex-

ponential from 370 μsec onwards: this suggests that ambipolar diffusion is the dominant loss process. This should be expected, since the ambipolar diffusion coefficient is large in helium at low pressure, and since the fundamental diffusion length is small ($\Lambda = 0.167$ cm for 8-mm tube diameter). Independent spectroscopic measurements of the recombination loss term, by the technique described in Sec. IV C, and of the source term, by the technique described previously by Delpech and Gauthier,[10] confirm that they are indeed negligible. Furthermore, it turns out that under our particular experimental conditions without microwave heating the last two terms on the right-hand-side of Eq. (5) cancel almost exactly each other during the whole of the afterglow period of interest. Cancellation is not as good during microwave heating as the source is practically unaffected while the recombination term is strongly reduced, but one may still write to a very good approximation

$$\left(\frac{dn_e}{dt}\right)_{\text{meas}} \cong \left(\frac{dn_e}{dt}\right)_{\text{diff}} = -\frac{D_a(T_e)}{\Lambda^2} n_e \ . \tag{6}$$

From the measured exponential decay after 370 μsec, in the absence of microwave heating, one deduces

$$D_a p = 475 \pm 7 \text{ cm}^2 \text{ sec}^{-1} \text{ Torr} \ ,$$

in good agreement at 300 °K with what can be deduced from the accepted mobilities of the atomic and molecular helium ions and the atomic-to-molecular ionic conversion coefficient.[5,14] A detailed analysis shows that the concentration of molecular ions never exceeds 7% of total ionic concentration. To a sufficient approximation then $n_{He^+} \cong n_e$; this is confirmed by the low intensity of the observed molecular helium bands.

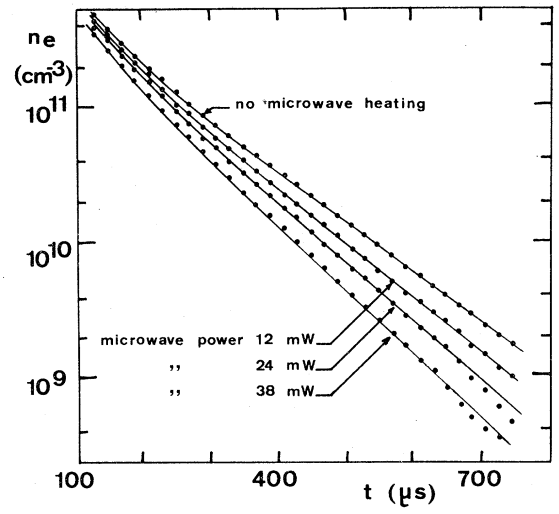

FIG. 3. Measured electron density on tube axis vs time for the four values of microwave heating power; measurements of the local slope of the curves yields the electron temperature through Eq. (9), as ambipolar diffusion is the dominant loss process.

One should also note that the fundamental diffusion length of the plasma container is much smaller than the energy relaxation length.[13] This ensures the homogeneity of the electron temperature over the tube, even in the presence of radially inhomogeneous heating.

Ambipolar diffusion being largely dominant, it follows that the radial profile of the electron density is given by

$$n_e(r) = n_e(0) J_0(2.405 r/R) \ , \tag{7}$$

where R is the tube radius and J_0 is the zero-order Bessel function. The axial electron density $n_e(0)$ is then related to the microwave measured spatial average value $\langle n_e \rangle$ by

$$n_e(0) = 2.31 \langle n_e \rangle \ . \tag{8}$$

Figure 3 shows n_e in the tube center.

Furthermore, according to ambipolar diffusion theory[14]

$$D_a(T_e) = \tfrac{1}{2} D_a(T_e = T_i)(1 + T_e/T_i) \ , \tag{9}$$

where T_i is the ion temperature, equal in this case to the gas temperature, i.e., 300 °K. A comparison of Eqs. (6) and (9) shows that a measurement of the slope, on a semilogarithmic plot, of the measured electron density versus time should yield a reliable evaluation of electron temperature.

We have already noted the fact that at times $t > 370$ μsec into the afterglow, without microwave heating, this slope corresponds to its expected value at 300 °K. Electron temperatures deduced from the measured slopes of the curves on Fig. 3 in presence of microwave heating are also in agreement within errors bars with their predicted values (see Table I).

Electron-density decay curves deviate slightly from an exponential at earlier times; this may be understood at least semiquantitatively by taking into account the fact that the free-electron gas is heated by the fast electrons produced by the electron-source term.[15] Similar phenomena have been extensively documented in cryogenic helium afterglows.[10,11] As the source term is very nearly independent of microwave heating under our experimental conditions, the electron-source heating term may be expected to be simply linearly additive to the microwave heating term, which is itself

TABLE I. Computed and measured electron temperature increments due to microwave heating.

Microwave heating (mW)	Computed electron temperature increment (°K)	Measured electron temperature increment (°K)
12	55	50 ± 6
24	110	109 ± 8
38	174	163 ± 11

independent of T_e. Figure 4 shows that this interpretation is coherent. The ambipolar diffusion time constants have been determined from the local slopes of the $\log_{10} n_e$-vs-time curves, and the electron temperatures from Eqs. (6) and (9); the unperturbed electron temperature $T_e - (\Delta T_e)_{\text{microw}}$, averaged over the four microwave heating powers (0, 12, 24, and 38 mW), has been plotted as a function of time.

In conclusion then, the measured electron temperature is well represented by

$$T_e = (\Delta T_e)_{\text{microw}} + (\Delta T_e)_{\text{source}} + 300\,^\circ\text{K} , \qquad (10)$$

where $(\Delta T_e)_{\text{microw}}$ is experimentally related to the microwave heating power (see Table I) and where

$$(\Delta T_e)_{\text{source}}(^\circ\text{K}) = \begin{cases} 628\exp(-t/500) - 300 \\ \quad \text{for } 150 < t < 370\ \mu\text{sec}, \\ 0 \text{ for } t \geq 370\ \mu\text{sec}. \end{cases} \qquad (11)$$

Systematic and statistical errors in the electron temperature as given by Eq. (10) should not exceed ±4%.

B. Excited-states populations

The light emitted on a given transition, at a given electron temperature, should be proportional to some power γ of the electron density. Electron temperature being uniform, the radial profile of the light emitted on the line under consideration, using Eq. (7), will be given by

$$I(r,t) = I(0,t)[J_0(2.405r/R)]^\gamma . \qquad (12)$$

Figure 5 shows the decay of a few lines belonging to the $p^3D - 2^3P$ series in the absence of microwave heating. For comparison, the corresponding evolution of the square of the electron density is also shown. The exponent γ is seen to lie between $\gamma = 2$ (for $p = 14$) and $\gamma = 2.35$ (for $p = 3$). This is of great practical advantage, as absolute

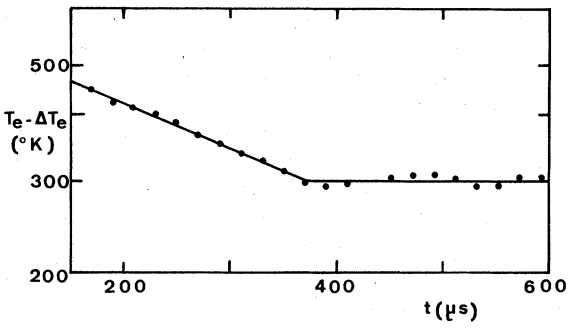

FIG. 4. Difference between the electron temperature deduced from Fig. 3 and the measured temperature increments due to microwave heating, averaged over the four different microwave heating powers. Solid line corresponds to $(\Delta T_e)_{\text{source}} + 300\,^\circ\text{K}$, as given by Eq. (11).

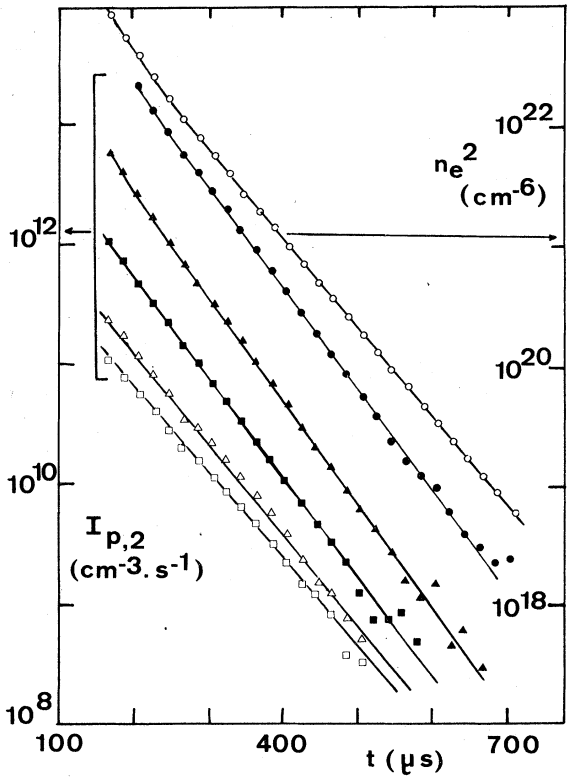

FIG. 5. Time dependence of the square of the electron density compared with the absolute intensity of selected lines: ●, 3^3D-2^3P; ▲, 6^3D-2^3P; ■, 9^3D-2^3P; △, 12^3D-2^3P; □, 14^3D-2^3P.

light intensity measurements yield a spatial average $\langle I(r,t)\rangle$ along a tube diameter. Now if $2 \leq \gamma \leq 2.5$ we may write

$$I(0,t) \cong 2.23\langle I(r,t)\rangle \ , \tag{13}$$

and we obtain the light intensity on the tube radius with a systematic error below 4.5%. The quartz tube exhibits a weak, broad band fluorescence in the blue, which decays slowly during the afterglow; its contribution was eliminated by double synchronous detection.

Spontaneous transition probabilities are well known for the helium atom[16] and absolute light intensity measurements yield directly the population density of the upper level involved in the transition.

The logarithm of the population density of the p^3D levels on tube axis is plotted in Fig. 6 against ionization energy at three different times in the afterglow. The independently measured electron densities and temperatures are also indicated, as well as the corresponding predicted population densities in the collisional radiative model[1] where the third body is an electron. However, one should already note that while the agreement may seem fair in order of magnitude, the experimental distribution of excited levels is much flatter than predicted, and does not show a hump around levels $p = 7$ to 10: this should not be too surprising in a

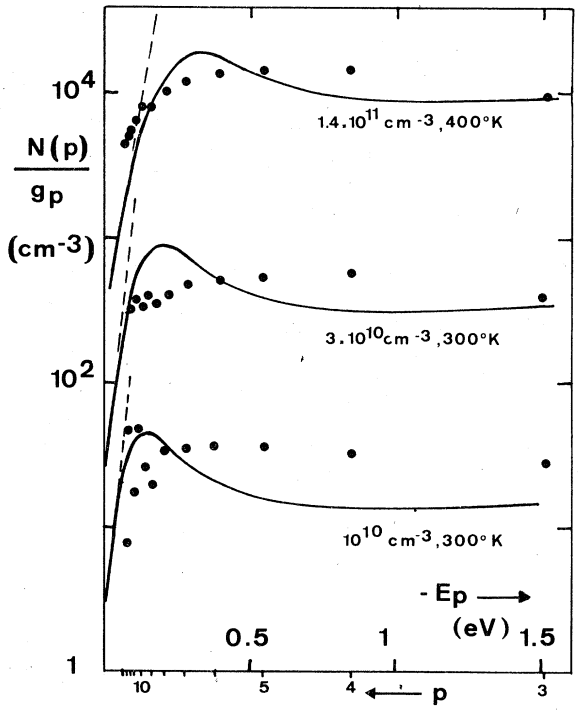

FIG. 6. Reduced populations of He(p^3D) levels; solid curves correspond to CR theory of I.

classical approximation; the sublevels of different orbital quantum number l may not be in thermal equilibrium for various reasons, at such low electron densities, and furthermore electron-neutral collisions should be expected to play a role. We shall examine this last point in more detail in Sec. IV C.

C. Determination of the electron-He^+ recombination rate coefficient

As mentioned in the Introduction, CR recombination with a neutral atom as a stabilizing third body should become important near 2 Torr, 300–500 °K, when the electron density is below a few 10^{10} cm^{-3}. To a good approximation, the rate coefficient α_{e0} of CR recombination simultaneously stabilized by electrons and neutral atoms should simply be the sum of the rate coefficient for collisional stabilization by neutrals α_0 and the electron CR rate coefficient α_e:

$$\alpha_{e0} = \alpha_e + \alpha_0 \ , \tag{14}$$

since it may be fairly assumed that the relative distribution of the excited levels which contribute substantially to the recombination process (i.e., around the bottleneck) does not depend significantly on the details of the collision processes,[17] and since the electron and neutral temperatures are in a ratio of order unity.

The electron-stabilized CR recombination rate coefficient for He^+ was computed in I. It is

$$\begin{aligned}\alpha_e^{(\mathrm{theor})}\ (\mathrm{cm^3\,sec^{-1}}) = {} & 1.55\times10^{-10}T_e^{-0.63} \\ & +6.0\times10^{-9}T_e^{-2.18}n_e^{0.37} \\ & +3.8\times10^{-9}T_e^{-4.5}n_e \ ,\end{aligned} \tag{15}$$

with T_e in °K and n_e in cm^{-3}.

Theoretical estimates for the neutral-stabilized recombination rate coefficient for He^+ in helium at 2 Torr, 300 °K range from

$$\alpha_0\ (\mathrm{cm^3\,sec^{-1}}) = 3.8\times10^{-5}T_e^{-2.5} \ , \tag{16a}$$

in the simple theory of Thomson, to

$$\alpha_0\ (\mathrm{cm^3\,sec^{-1}}) = 2.4\times10^{-4}T_e^{-2.5} \ , \tag{16b}$$

in the theory of Pitaevski. The results of both theories are reported by Bates and Khare[6] and their own predictions are well represented in our temperature and density range by

$$\alpha_0\ (\mathrm{cm^3\,sec^{-1}}) = 1.2\times10^{-4}T_e^{-2.5} \ . \tag{16c}$$

While the absolute values range over almost an order of magnitude, the basic functional dependences are the same in these conceptually different theories.

Under our experimental conditions of relatively

low electron and neutral densities, it seems reasonable to assume that direct nonradiative population of the $p=2$ states is negligible. The experimental rate coefficient of recombination $\alpha^{(\mathrm{expt})}$ into the $p=2$ states can then be found[18-20] by summing all radiative deexcitations to the $p=2$ states:

$$\left(\frac{dn_e}{dt}\right)_{\mathrm{rec}} = \alpha^{(\mathrm{expt})} n_e n_{\mathrm{He}^+} = \sum_{p=3}^{\infty} I_{p,2} \ , \tag{17}$$

where $I_{p,2}$ is the measured absolute intensity of all radiation from levels with principal quantum number p to levels with quantum number 2, summed over the six ($p=2$) spectral series of helium, and expressed in number of photons per cm^3 and per second. The series is found to converge quite rapidly and it is sufficient to truncate it at $p=7$.

One should bear in mind that there may be untrapped radiative pathways in the vacuum ultraviolet from excited, $p>2$ atomic states to the fundamental He (1^1S) state [for example, by formation of a He_2 ($p^1\Sigma$) state followed by radiative deexcitation to the fundamental dissociative He_2 ($X^1\Sigma$) state]. Such processes were neglected in the theory of I; in consequence $\alpha^{(\mathrm{expt})}$ defined by Eq. (17) is directly comparable to our theoretical predictions but may be different from the e-He^+ recombination rate coefficient into the fundamental He (1^1S) state. We expect this difference to be negligible at helium pressures of a few Torrs.

As reported in Sec. III, we have made precise measurements of the light intensities $I_{p,2}$; the electron density n_e and temperature T_e were deduced from microwave diagnostics, and $n_{\mathrm{He}^+} \cong n_e$. The recombination rate coefficient $\alpha^{(\mathrm{expt})}$ on tube axis deduced through Eq. (17) when no microwave heating field is applied is shown in the top part of Fig. 7 (full circles) as a function of electron density which decays in the afterglow from 3×10^{11} to 3×10^{9} cm^{-3} [the corresponding time in the afterglow can be read from Fig. 3 and the electron temperature may then be deduced from Eqs. (10) and (11)]. Error bars correspond to possible systematic errors in the measurement of the relevant parameters, and random errors are indicated by the scatter of the data points.

Also shown on Fig. 7 (triangles) is the theoretically predicted $\alpha_e^{(\mathrm{ther})}$ given by Eq. (15); the length of the error bars corresponds to the estimated possible systematic uncertainties in n_e and T_e. It can be seen that $\alpha^{(\mathrm{expt})}$ and $\alpha_e^{(\mathrm{ther})}$ are significantly different, and that the difference increases as n_e decreases. The situation remains qualitatively similar in presence of microwave heating fields;

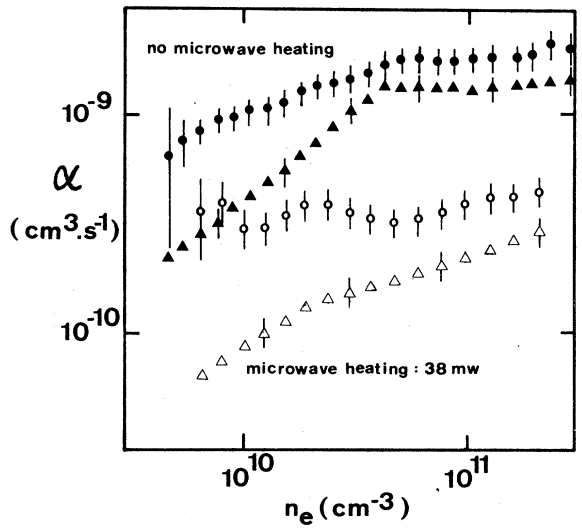

FIG. 7. Measured recombination rate coefficient (dots) and theoretical contribution of the electrons (triangles) computed from the measured electron density and temperature [Eq. (15)] without microwave heating (full symbols) and with 38-mW microwave heating power (open symbols).

the case of 38-mW heating power is also shown on Fig. 7.

These observations are consistent with the expected contribution of stabilization by neutrals to the global recombination phenomenon, and consequently to its rate coefficient α; we have thus constructed the difference

$$\alpha_0^{(\mathrm{expt})} = \alpha^{(\mathrm{expt})} - \alpha_e^{(\mathrm{ther})} \tag{18}$$

between the experimental recombination rate coefficient $\alpha^{(\mathrm{expt})}$ and the theoretically predicted rate for electron-stabilized CR recombination $\alpha_e^{(\mathrm{ther})}$, using independently measured values of n_e and T_e. No dependence of $\alpha_0^{(\mathrm{expt})}$ on electron density was found over almost two decades. On the other hand, $\alpha_0^{(\mathrm{expt})}$ exhibits a strong electron temperature dependence; the 80 experimental points obtained with and without microwave heating have been reduced into the nine rectangles shown in logarithmic coordinates on Fig. 8. The corresponding weighted regression line yields

$$\alpha_0^{(\mathrm{expt})}\ (\mathrm{cm}^3\,\mathrm{sec}^{-1}) = 3.5\times10^{-5} T_e^{-1.9} \ , \tag{19}$$

in reasonable agreement, both in order of magnitude and in electron temperature dependence, with the theoretical predictions of neutral stabilized CR recombination.

Conversely, we have constructed the difference

$$\alpha_e^{(\mathrm{expt})} = \alpha^{(\mathrm{expt})} - \alpha_0^{(\mathrm{expt})} \ , \tag{20}$$

with $\alpha_0^{(\mathrm{expt})}$ given by Eq. (19). This has been plotted on Fig. 9 in the "universal coordinates" X and Y

introduced in I. This procedure yields of course experimental points in average agreement with the "universal curve" which is the locus of $\alpha_e^{(\mathrm{ther})}$ in the XY plane. However, it is important to note the relatively small scatter of the experimental results over this wide range of experimental conditions; furthermore, the distances of the points to the theoretical curve (residuals) do not show any statistically significant dependence on any identified parameter.

As the only two independent variables are n_e and T_e, the procedure just described amounts simply to a two-dimensional nonlinear regression of the raw experimental data $\alpha^{(\mathrm{expt})}$ to the functional form

$$\alpha = BT_e^{-\beta} + C\alpha_e \ ,$$

where B and C are independent of n_e and T_e, and α_e is given by Eq. (15) and is thus dependent on both T_e and n_e. While the choice of this functional form is to some extent arbitrary, it is directly suggested by the theoretical considerations leading to Eq. (14), and it is confirmed by the fact that there appears to be an electron-density–independent experimental contribution to the total recombination rate coefficient; it is also coherent with our experimental results with infrared irradiation (Sec. IV D below). The regression yields $B = 3.5 \times 10^{-5}$ (cgs units), $\beta = 1.9$ and $C = 1$. The total electron-He^+ recombination coefficient in helium gas at 300 °K, 2.03 Torr is thus well represented under our experimental conditions by

$$\alpha^{(\mathrm{expt})}\ (\mathrm{cm^3\,sec^{-1}}) = 3.5\times10^{-5}T_e^{-1.9} + 6.0\times10^{-9}T_e^{-2.18}n_e^{0.37} + 3.8\times10^{-9}T_e^{-4.5}n_e \ . \qquad (21)$$

Equation (21) fits our experimental data within error bars (see Figs. 8 and 9) and appears to support experimentally the presence of neutral-stabilized CR recombination of the atomic ion He^+; we shall see in Sec. IV D that this interpretation is also supported by our results with infrared irradiation. However, to confirm the presence of neutral-stabilized recombination, it would have been extremely useful to vary significantly the neutral density, i.e., the gas pressure. At pressures below 2 Torr, it was not possible with our experimental system to obtain a discharge of the outstanding stability and reproducibility which are absolutely necessary for such spectroscopic studies. On the high-pressure side, a series of experiments was performed at a gas pressure of 5.15 Torr; while reproducibility was good, absolute spectroscopic evaluation of the recombination rate coefficient $\alpha^{(\mathrm{expt})}$ was not possible, as the concentration of the molecular ion He_2^+ was large and could not be measured absolutely. The relative

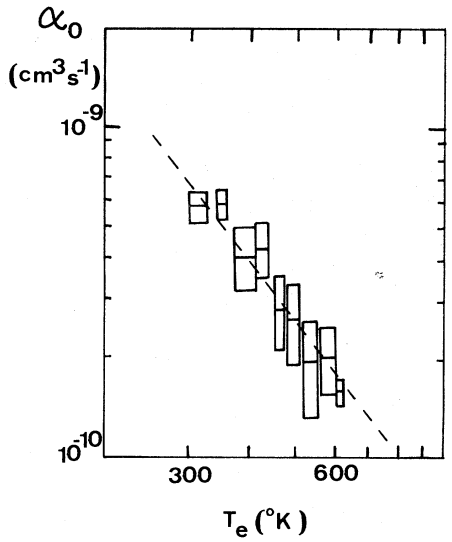

FIG. 8. Electron temperature dependence of the difference α_0 between the experimental recombination rate coefficient and the theoretically predicted rate for electron-stabilized CR recombination using independently measured values of n_e and T_e [Eq. (18)].

rate coefficient could however by evaluated and its general behavior with electron density was in good qualitative agreement with the results at 2 Torr reported in this section after proper scaling.

D. Experimental results with CO_2 laser irradiation

It was first experimentally verified that at a given 10.6-μm photon flux Φ and electron density

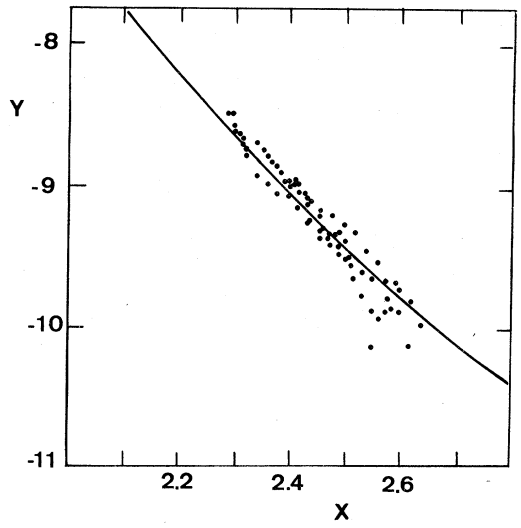

FIG. 9. Electron density and temperature dependence of $\alpha_e^{(\mathrm{expt})}$ [Eq. (20)] plotted in the universal coordinates introduced in I: $X = \log_{10}[(n_e/10^{10})^{-0.258}T_e]$, $Y = \log_{10}[(n_e/10^{10})^{0.163}\alpha]$, compared with the universal curve computed from electron-stabilized CR recombination theory with Mansbach and Keck rate coefficients.

n_e and at constant neutral pressure all energy levels and observable sublevels of principal quantum number $p < 11$ exhibited the same relative quenching Q_p, as predicted by CR theory (see Sec. II).

Light intensities for transitions originating from the high quantum levels were too weak to yield statistically significant Q_p values. On the contrary, the quenchings of the lower levels (which emit most afterglow light) were readily measured; as they were all found to behave similarly, as predicted by theory, we only report here results obtained on the 3^3D-2^3P line at 5876 Å; its relative quenching [defined by Eq. (3)] will be denoted Q_3 in what follows.

The results for electron temperatures between 300 and 380 °K and for electron densities above 6×10^{10} cm^{-3} are shown in Fig. 10. They are in good agreement with the predictions of electron-stabilized CR theory with Mansbach and Keck transition rates over the corresponding range of electron temperatures [see Eq. (4)]. They are significantly larger than predicted by the same theory using Gryziński's transition rates (broken line).

Figure 11 shows the relative quenching Q_3 over the whole range of electron densities covered in this experiment at electron temperatures between 300 and 380 °K, at a single infrared power density of 300 W cm^{-2}. As predicted, the quenching becomes independent of electron density at low electron density; we interpret this observation as corresponding to the onset of neutral-dominated transfer, and it occurs at electron densities between 6×10^{10} and 10^{11} cm^{-3}.

As quenchings are defined as relative quantities, measurements were also possible at 5.15 Torr, with the only limitation that light intensity, even

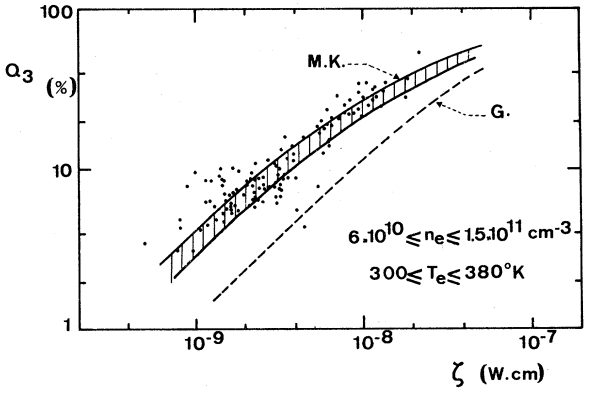

FIG. 10. Relative quenching of the 3^3D level vs the ratio ζ of ir power flux over electron density and theoretical previsions of electron stabilized CR recombination using Mansbach and Keck (MK) rate coefficients for T_e between 300 and 380 °K (dashed zone) and with Gryziński (G) rate coefficients for $T_e = 300$ °K (dashed line).

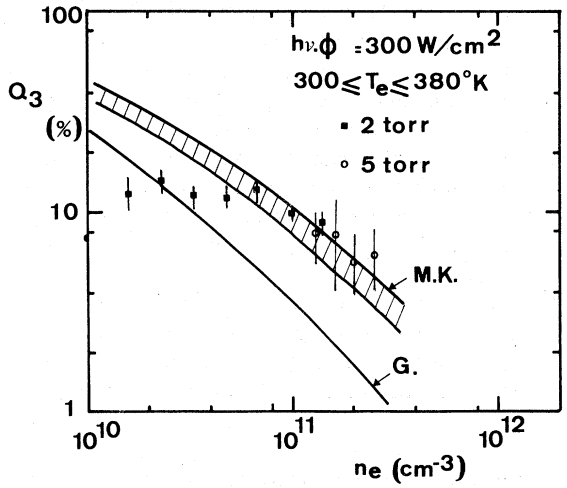

FIG. 11. Relative quenching of the 3^3D level vs electron density with 300-W/cm^2 ir power and theoretical previsions of electron-stabilized CR recombination using Mansbach and Keck (MK) rate coefficients for T_e between 300 and 380 °K (dashed zone) and with Gryziński (G) rate coefficients for $T_e = 300$ °K (Solid line). Saturation of the quenching at low electron densities corresponds to the onset of neutral-dominated transfers.

on the 5876-Å line, now becomes too weak to allow measurements at electron densities below 10^{11} cm^{-3}. However, results obtained for $n_e > 10^{11}$ cm^{-3} are also shown on Fig. 11; they extend to higher densities and they confirm the good agreement at high electron densities between our experiments and the collisional-radiative electron-stabilized theory using Mansbach and Keck collisional transfer rates.

V. CONCLUSION

We have presented detailed spectroscopic measurements of light emission and excited level populations in a thermalized plasma of central electron density from 5×10^9 to 3×10^{11} cm^{-3} and electron temperature from 300 to 600 °K, at a gas temperature of 300 °K and at a pressure of 2.03 Torr. Electron density and temperature were obtained by microwave interferometry independently of optical measurements, and an absolute comparison was thus possible between experiment and collisional-radiative theory. Interpretation of the experimental results has been considerably simplified by choosing experimental conditions such that ambipolar diffusion was the dominant electron-loss mechanism, and by application of well-controlled perturbation techniques of the free electron population and of the Rydberg states of neutral helium. In contrast, it should be noted that in previous work the measured population

densities were used to obtain electron temperature[20,21] or electron temperature and density, or that the collisional transition rates were adjusted so as to obtain agreement between calculated and measured population densities[22]; furthermore, previous studies (except in the case of Collins *et al.*[20]) were performed at higher electron densities and/or temperatures.

All our experimental data are consistent with a collisional-radiative (CR) recombination scheme with simultaneous stabilization by collisions with free electrons and with neutral helium atoms. They establish the fact that the Gryziński formalism[9] for electron-impact–induced transitions between bound Rydberg states of high principal quantum number overestimates seriously the probability of collisions with small energy transfer; this is independently confirmed by our study of the perturbation of the afterglow by infrared irradiation with a CO_2 laser: at electron densities around 10^{11} cm^{-3} and larger where electron collisions are dominant, the relative quenching of the recombination produced by photoionization of the $p \geq 11$ levels follows closely the predictions of a CR theory using Mansbach and Keck[2] rates, while it is in substantial disagreement with a similar theory using Gryziński rates.

The present study gives also the first experimental indications on what appears to be neutral-stabilized collisional-radiative recombination of an atomic ion, in this case He^+. An electron-ion recombination process governed by neutral atom collisions with a rate coefficient proportional to gas pressure has been previously reported for the He_2^+ ion[23]; neutral collisions appeared at least in part in connection with vibrational-rotational energy transfers[24] and were thus presumably a characteristic molecular feature. In the present case, various mechanisms may be invoked for excitation transfer between atomic excited states and for stabilization of the recombination; in addition to collisional transfers, one may, for example, envision curve crossings between diabatic He_2 states and the He_2^+ ion potential curve near its dissociation limit.[25] A detailed study of these individual mechanisms appears now to be possible both theoretically[26] and experimentally[27] and would be of interest.

ACKNOWLEDGMENTS

It is a pleasure to acknowledge several helpful discussions with Dr. L. Goldstein, with members of the Groupe d'Electronique dans les Gaz at Orsay, and with Dr. W. E. Wells. Dr. J.-P. Moy helped in the design of the CO_2 laser and the associated ir optics, and M. J.-P. Puissant in its practical implementation. This work was supported by Direction des Recherches et Moyens d'Essais under contract No. 74/34/418.

*Present address: Groupe de Recherches sur l'Energétique des Milieux Ionisés, Université d'Orléans, 45045 Orleans, France.

[1]J. Stevefelt, J. Boulmer, and J.-F. Delpech, Phys. Rev. A 12, 1246 (1975).
[2]P. Mansbach and J. Keck, Phys. Rev. 181, 275 (1969).
[3]D. R. Bates, A. E. Kingston, and R. W. P. McWhirter, Proc. R. Soc. A 267, 297 (1962); and 270, 155 (1962).
[4]L. C. Johnson and E. Hinnov, J. Quant. Spectrosc. Radiat. Transfer 13, 333 (1973).
[5]J.-F. Delpech, J. Boulmer, and J. Stevefelt, in *Advances in Electronics and Electron Physics*, edited by L. Marton (Academic, New York, 1975), Vol. 39.
[6]D. R. Bates and S. P. Khare, Proc. Phys. Soc. Lond. 85, 231 (1965).
[7]J. P. Kaplafka, H. Merkelo and L. Goldstein, Appl. Phys. Lett. 15, 113 (1969); and 19, 197 (1971).
[8]M. J. Seaton, Mon. Not. R. Astron. Soc. 119, 81 (1964).
[9]M. Gryziński, Phys. Rev. 115, 374 (1959).
[10]J.-F. Delpech and J.-C. Gauthier, Phys. Rev. A 6, 1932 (1972).
[11]C. Sol, J. Boulmer, and J.-F. Delpech, Phys. Rev. A 7, 1023 (1973).
[12]J. M. Anderson and L. Goldstein, Phys. Rev. 100, 1037 (1955); and 102, 933 (1956).
[13]J.-C. Gauthier and J.-F. Delpech, Phys. Fluids 18, 1467 (1975).
[14]H. J. Oskam, Philips Res. Rep. 13, 335 (1958); and 13, 401 (1958).
[15]J. C. Ingraham and S. C. Brown, Phys. Rev. 138, A1015 (1965).
[16]W. L. Wiese, M. W. Smith, and B. M. Glennon, *Atomic Transition Probabilities*, Natl. Bur. Stand. Special Report No. NSRDS-NBS 4 (U.S. GPO, Washington, D.C., 1966), Vol. 1.
[17]D. R. Bates, Comments At. Mol. Phys. 5, 89 (1976).
[18]F. Robben, W. B. Kunkel, and L. Talbot, Phys. Rev. 132, 2363 (1963).
[19]J. Stevefelt and F. Robben, Phys. Rev. A 5, 1502 (1972).
[20]C. B. Collins, H. S. Hicks, W. E. Wells, and R. Burton, Phys. Rev. A 6, 1545 (1972).
[21]E. Hinnov and J. G. Hirschberg, Phys. Rev. 125, 795 (1962).
[22]L. C. Johnson and E. Hinnov, Phys. Rev. 187, 143 (1969).
[23]J. Berlande, M. Chéret, R. Deloche, A. Gonfalone, and C. Manus, Phys. Rev. A 1, 887 (1970).
[24]J. Boulmer, J. Stevefelt, and J.-F. Delpech, Phys. Rev. Lett. 33, 1248 (1974).
[25]J. Stevefelt, Phys. Rev. A 8, 2507 (1973).
[26]J. S. Cohen, Phys. Rev. A 13, 99 (1976).
[27]J.-C. Gauthier, F. Devos, and J.-F. Delpech, Phys. Rev. A 14, 2182 (1976).